THE JOURNAL OF BIOLOGICAL CHEMISTRY VOL. 289, NO. 40, pp. 28006–28018, October 3, 2014

Rapid Binding of Plasminogen to Streptokinase in a Catalytic Complex Reveals a Three-step Mechanism*

Received for publication, June 11, 2014, and in revised form, August 6, 2014 Published, JBC Papers in Press, August 19, 2014, DOI 10.1074/jbc.M114.589077

Ingrid M. Verhamme and Paul E. Bock[1]

From the Department of Pathology, Microbiology, and Immunology, Vanderbilt University School of Medicine, Nashville, Tennessee 37232

Background: We previously showed that plasmin binding to streptokinase is a three-step mechanism with a slow off-rate.
Results: Using rapid kinetics and equilibrium binding, we defined the unknown mechanism of plasminogen binding to streptokinase.
Conclusion: Encounter complex formation and conformational tightening are weakened in the three-step binding mechanism.
Significance: The results define the molecular basis for plasminogen displacement by plasmin in complexes with streptokinase.

Rapid kinetics demonstrate a three-step pathway of streptokinase (SK) binding to plasminogen (Pg), the zymogen of plasmin (Pm). Formation of a fluorescently silent encounter complex is followed by two conformational tightening steps reported by fluorescence quenches. Forward reactions were defined by time courses of biphasic quenching during complex formation between SK or its COOH-terminal Lys^{414} deletion mutant (SKΔK414) and active site-labeled [Lys]Pg ([5-(acetamido)fluorescein]-D-Phe-Phe-Arg-[Lys]Pg ([5F]FFR-[Lys]Pg)) and by the SK dependences of the quench rates. Active site-blocked Pm rapidly displaced [5F]FFR-[Lys]Pg from the complex. The encounter and final SK·[5F]FFR-[Lys]Pg complexes were weakened similarly by SK Lys^{414} deletion and blocking of lysine-binding sites (LBSs) on Pg kringles with 6-aminohexanoic acid or benzamidine. Forward and reverse rates for both tightening steps were unaffected by 6-aminohexanoic acid, whereas benzamidine released constraints on the first conformational tightening. This indicated that binding of SK Lys^{414} to Pg kringle 4 plays a role in recognition of Pg by SK. The substantially lower affinity of the final SK·Pg complex compared with SK·Pm is characterized by a ~25-fold weaker encounter complex and ~40-fold faster off-rates for the second conformational step. The results suggest that effective Pg encounter requires SK Lys^{414} engagement and significant non-LBS interactions with the protease domain, whereas Pm binding additionally requires contributions of other lysines. This difference may be responsible for the lower affinity of the SK·Pg complex and the expression of a weaker "pro"-exosite for binding of a second Pg in the substrate mode compared with SK·Pm.

The serine proteinase plasmin (Pm)[2] is primarily known for its role in dissolving fibrin thrombi (1). It also causes cell surface remodeling, signaling, and cancer progression (2). Proteolytic activation of the zymogen plasminogen (Pg) by tissue plasminogen activator and urokinase-type plasminogen activator differs from conformational activation by the non-enzymatic streptococcal pathogenicity factor streptokinase (SK). We studied SK from *Streptococcus dysgalactiae* subsp. *equisimilis* because of its 90% homology with phylogenetic cluster 1SKs from the human host-specific, virulent *Streptococcus pyogenes* (3). *S. dysgalactiae* subsp. *equisimilis*, which is generally opportunistic in horses, also causes severe human infections such as bacteremia, pneumonia, endocarditis, arthritis, and streptococcal toxic shock syndrome (4, 5).

The Pg activation mechanism by SK is unique (6–8). Stoichiometric binding of SK to Pg and Pm forms catalytically active SK·Pg* and SK·Pm complexes that bind Pg as a substrate in SK·Pg*·Pg and SK·Pm·Pg assemblies and cleave Arg^{561}-Val^{562} in the Pg protease domain to form Pm (6, 8–14). Conformational activation of Pg in the catalytic SK·Pg* complex by the molecular sexuality mechanism involves insertion of the NH_2-terminal Ile^1-Ala^2 residues of SK into the binding cleft of the Pg protease domain (9, 11, 12, 15–17). Ile^1 binds Pg Asp^{194} (chymotrypsinogen numbering), causing expression of the substrate-binding site and formation of the oxyanion hole (15, 16, 18, 19). The mechanism is also valid for conformational prothrombin activation by staphylocoagulase and von Willebrand factor-binding protein from *Staphylococcus aureus* (20, 21). This mechanism allows group A and C streptococci to hijack Pg in the human fibrinolytic system by quorum sensing-induced secretion of SK. This results in localized plasmin generation for dissolution of host fibrin barriers and facilitated bacterial spreading (22–25).

In our unified model, the conformationally activated SK·Pg* complex binds Pg as a substrate and cleaves it to Pm. This is the

* This work was supported, in whole or in part, by National Institutes of Health Grant R01 HL056181 from the NHLBI (to P. E. B.).
[1] To whom correspondence should be addressed: Dept. of Pathology, Microbiology, and Immunology, Vanderbilt University School of Medicine, C3321A Medical Center North, Nashville, TN 37232-2561. Tel.: 615-343-9863; Fax: 615-322-1855; E-mail: paul.bock@vanderbilt.edu.
[2] The abbreviations used are: Pm, plasmin; SK, streptokinase; SKΔK414, SK lacking the COOH-terminal Lys^{414} residue; nSK, native streptokinase; Pg, plasminogen; [Glu]Pg, intact native plasminogen; [Lys]Pg, native Pg lacking the N-terminal 77 residues; [Lys]Pg*, the conformationally activated form of Pg; FFR-CH_2Cl, D-Phe-Phe-Arg-CH_2Cl; FFR-Pm, Pm inhibited with D-Phe-Phe-Arg-CH_2Cl; [5F]FFR-[Lys]Pg, [5-(acetamido)fluorescein]-D-Phe-Phe-Arg-[Lys]Pg; [5F]FFR-[Glu]Pg, [5-(acetamido)-fluorescein]-D-Phe-Phe-Arg-[Glu]Pg; 6-AHA, 6-aminohexanoic acid; Pg*, nonproteolytically activated form of the plasminogen zymogen; LBS, lysine-binding site; PAN, plasminogen, apple, nematode; K, kringle; [5F], 5-fluorescein; Fbg, fibrinogen; $[SK]_o$, total SK concentration.

trigger step in a self-limiting mechanism (6–8). After 1 SK eq of Pm is formed, it displaces Pg from the SK·Pg* complex to form the tight SK·Pm catalytic complex (with dissociation constant (K_D) of 12 pM (26, 27)) that cleaves the remaining free Pg to Pm in a second catalytic cycle, the bullet cycle (6). In the SK·Pm complex, the three SK β-grasp domains rearrange from a beads-on-a-string conformation (28) to a crater surrounding the Pm active site (19). This forms a novel exosite for substrate Pg binding (19, 26).

[Glu]Pg, the circulating form of Pg, has an NH_2-terminal plasminogen, apple, nematode (PAN) module, five kringles (K1–K5) with lysine-binding sites (LBSs), and a COOH-terminal serine protease domain (29–31). K1, K2, K4, and K5 bind lysine analogs and small aromatic anionic and cationic ligands (32). K1, K4, and K5 also bind COOH-terminal lysines on fibrin and other proteins (33–38). In the compact [Glu]Pg, the NH_2-terminal PAN module occupies the LBS on K5, and in this spiral α-form, [Glu]Pg activation is inefficient (27, 39–43). Cleavage of the 77-residue PAN module by Pm converts [Glu]Pg to [Lys]Pg with a partially extended β-conformation that exposes kringle LBSs and is readily activated (6, 44–47). Occupying these LBSs with the lysine analog 6-aminohexanoic acid (6-AHA) fully extends [Lys]Pg to the γ-form (39, 43). SK binds weakly to [Glu]Pg in the absence and presence of 6-AHA, whereas SK binding to [Lys]Pg is tighter due in part to the interaction of the COOH-terminal Lys^{414} residue of SK with exposed LBSs on kringle domains in [Lys]Pg (48). This interaction is weakened ~13–20-fold by blocking the LBSs with 6-AHA (27, 48). 6-AHA binds isolated kringles K1, K4, and K5 (30, 32, 49, 50), whereas benzamidine binds K1, K2, and K5 (32, 51, 52) and only partially extends [Glu]Pg and [Lys]Pg to the β-conformation (39, 43). K4 and K5 of [Glu]Pg were shown to bind 6-AHA cooperatively (53), which may be of importance in interpreting differences in binding of SK lysines to Pg and Pm. In this study, we used 6-AHA and benzamidine to study differential effects of LBS occupation on the formation of a stabilized SK·Pg complex.

Allosteric linkage between the protease active site and its exosite(s) allows investigating equilibrium binding of ligands to serine proteases labeled at their active sites with fluorescent probes (54–56). Active site labeling of the conformationally activated zymogens plasminogen and prothrombin (27, 57) provides the advantage of studying ligand binding uncoupled from catalytic activity. Introducing the fluorescent label 5-fluorescein ([5F]) and a tripeptide chloromethyl ketone in the Pm active site (FFR-Pm) does not affect the affinity for SK, whereas labeled [Glu]Pg and [Lys]Pg analogs bind SK with ~5-fold lower affinity than the native proteins (26, 48, 58). We compared the binding kinetics of labeled Pg and Pm that have their active sites similarly locked in a substrate-binding conformation by the tripeptide chloromethyl ketone.

Here we explore for the first time the steps on the pathway of SK binding to Pg and identify critical differences with Pm binding (59) that are the basis for the ~4,000-fold lower affinity of [5F]FFR-[Lys]Pg for SK (27). Stopped-flow kinetics of SK binding to labeled [Lys]Pg and [Glu]Pg defined the forward reactions of complex stabilization. Reverse reactions were studied by competitive displacement of labeled [Lys]Pg by active site-blocked FFR-Pm in the complex with SK. Forward and reverse reactions were biexponential, and overall off-rates were fast, requiring stopped-flow monitoring. Parameters from numerical integration of full forward and reverse time traces were consistent with those from the SK dependences of the forward rates of these conformational changes. This approach allowed a comparison of the elementary reaction steps in the sequence of SK·Pg* and SK·Pm formation. The data support a three-step mechanism of encounter complex formation followed by two tightening conformational steps as shown previously for SK·Pm (59) but with dramatic decreases in affinity of the encounter complex and ~10–40-fold increases in off-rates for both conformational steps. Based on selective blocking of LBSs on Pg and Pm and binding experiments with SK lacking Lys^{414}, we propose that the SK·Pg* complex is stabilized by SK Lys^{414} binding to LBSs on Pg and non-LBS interactions of SK within the Pg catalytic domain. These interactions are also present in the SK·Pm complex; however, additional contributions of SK lysines other than Lys^{414} may be partially responsible for the substantially tighter SK-Pm interaction.

EXPERIMENTAL PROCEDURES

Protein Purification and Characterization—[Glu]Pg carbohydrate form 2 was purified from human plasma and activated to [Lys]Pg and [Lys]Pm (Pm) as described (8, 26, 27, 60, 61). Pm was purified by affinity chromatography on soybean trypsin inhibitor-agarose and dialyzed against 5 mM HEPES, 0.3 M NaCl, 10 mM 6-AHA, 1 mg/ml PEG 8000 at pH 7.0 and 4 °C. The active Pm concentration (~90%) was determined by active site titration with fluorescein mono-*p*-guanidinobenzoate (62). Pm (10–15 μM) was covalently inactivated with a 5-fold molar excess of D-Phe-Phe-Arg-CH_2Cl (FFR-CH_2Cl) in 0.1 M HEPES, 0.3 M NaCl, 1 mM EDTA, 10 mM 6-AHA, 1 mg/ml PEG 8000, pH 7.0 buffer at 25 °C for 30–60 min until hydrolysis of D-Val-Leu-Lys-*p*-nitroanilide was undetectable. Excess inhibitor was removed by dialysis against >250 volumes of 50 mM HEPES, 0.3 M NaCl, 1 mM EDTA, pH 7.0 at 4 °C. Native SK (nSK; Diapharma) was purified from outdated therapeutic SK from the *S. dysgalactiae* subsp. *equisimilis* strain H46A (26, 27). Recombinant wild-type SK (WT-SK) and the SKΔK414 and SKΔ(R253–L260)ΔK414-His_6 mutants were prepared as published (48, 63). Proteins were quick frozen in 2-propanol/dry ice and stored at −80 °C. Protein concentrations were determined by absorbance at 280 nm using the following absorption coefficients ($(mg/ml)^{-1}$ cm^{-1}) and molecular weights: [Glu]Pg, 1.69 and 92,000; [Lys]Pg, 1.69 and 84,000; Pm, 1.9 and 84,000 (47, 61, 64); SK and SKΔK414, 0.81 and 47,000 (65, 66); SKΔ(R253–L260)ΔK414-His_6, 0.78 and 49,213 (63).

Active Site Labeling of Pg—[Glu]Pg and [Lys]Pg were labeled at the active site as described previously (27, 58, 63). The SKΔ(R253–L260)ΔK414-His_6 mutant activates [Lys]Pg conformationally, but the complex does not readily cleave Pg to Pm, and the use of this SK construct for Pg labeling significantly increased the yield of labeled Pg and reduced the preparation time (63). Labeled Pg concentration and probe incorporation (~90%) were determined from the probe and protein absorbances in 6 M guanidine as described (48, 54, 55). Proteins were homogeneous by SDS gel electrophoresis.

Stopped-flow Kinetics of nSK, WT-SK, and SKΔK414 Binding to [5F]FFR-Pg—Complete progress curves of SK binding to labeled Pg were captured with an Applied Photophysics SX-18MV stopped-flow spectrofluorometer in single mixing mode with excitation at 500 nm and an emission cut-on filter (Melles-Griot) with 50% transmission at 515 nm. Changes in fluorescence intensity were measured for all the reactions, and for the interaction of native SK with [5F]FFR-[Lys]Pg in the absence of lysine analogs, changes in fluorescence anisotropy were also monitored. The reaction volume was 200 μl, the path length was 2 mm, and experiments were performed at 25 °C. Binding was studied under pseudo-first-order conditions (SK ≥5-fold over labeled Pg) in 50 mM HEPES, 0.125 M NaCl, 1 mM EDTA, 1 mg/ml PEG 8000, 1 mg/ml bovine serum albumin, 1 μM FFR-CH_2Cl, pH 7.4 in the absence and presence of 50 mM 6-AHA or in 50 mM HEPES, 0.075 M NaCl, 1 mM EDTA, 1 mg/ml PEG 8000, 1 mg/ml bovine serum albumin, 1 μM FFR-CH_2Cl, pH 7.4 containing 50 mM benzamidine to maintain constant ionic strength. Binding of nSK and SKΔK414 (0.050–18 μM) to [5F]FFR-[Lys]Pg (10–20 nM) was studied in all three buffer systems. Binding of WT-SK (0.050–10 μM) to [5F]FFR-[Lys]Pg (20 nM) in the absence of effectors was included as a control. Binding of native SK (0.1–6 μM) to [5F]FFR-[Glu]Pg (13 and 20 nM) was studied in the absence and presence of 50 mM 6-AHA. Averaged time traces (1,000 data points/trace and 10 traces for each SK concentration) of the decrease in fluorescence intensity or increase in anisotropy ranged from 0.4 to 50 s, depending on the SK concentration and the presence of effector. Averaged time traces of blank titrations containing buffer and SK only and buffer and [5F]FFR-Pg only were obtained to measure background light scattering and initial probe fluorescence, respectively, and to permit transformation of raw data into the fractional change in initial fluorescence ($(F_{obs} - F_o)/F_o = \Delta F/F_o$) or anisotropy ($(r_{obs} - r_o)/r_o = \Delta r/r_o$). Subtracting background scattering was critical as the signal-to-noise ratio for reactions with [5F]FFR-Pg (~25% quench and ~7.5% maximal scattering) was up to 5-fold smaller than that for reactions with [5F]FFR-Pm (~50% quench and ~6% maximal scattering) (59). Experiments were limited to labeled Pg concentrations up to 20 nM due to the lower solubility of the SK·Pg complex compared with that of SK·Pm, which resulted in a substantial increase in background scattering at Pg concentrations above ~40 nM. None of our previously published studies of SK binding and kinetics have used [Lys]Pg and [Glu]Pg concentrations exceeding 20 and 30 nM, respectively. Averaged time traces were analyzed using Equation 1.

$$\Delta F/F_0 = (F_0 - F_M)(A_1 e^{(-k_{obs\,1}\,t)} + (1 - A_1)e^{(-k_{obs\,2}\,t)}) + F_M \quad \text{(Eq. 1)}$$

where F_o is the starting fluorescence, F_M is the final fluorescence, A_1 is the fractional amplitude of the fast exponential component, $(1 - A_1)$ is the fractional amplitude of the slow exponential component, and $k_{obs\,1}$ and $k_{obs\,2}$ are the observed first-order rate constants for the fast and the slow conformational changes. The rate constants were analyzed as a function of the total SK concentration ($[SK]_o$) using Equation 2.

$$k_{obs1,2} = \frac{k_{lim\,1,2}[SK]_0}{K_1 + [SK]_0} + k_{off\,1,2} \quad \text{(Eq. 2)}$$

where K_1 is the dissociation constant for the SK·Pg encounter complex and $k_{lim\,1,2}$ and $k_{off\,1,2}$ are the limiting rates and the reverse rate constants for each conformational step, respectively.

Competitive Dissociation of [5F]FFR-[Lys]Pg from its Complex with nSK, WT-SK, and SKΔK414 by FFR-Pm—In stopped-flow experiments, [5F]FFR-[Lys]Pg and SK or SKΔK414 were preincubated in the dark for 5 min at 25 °C and loaded in one syringe. FFR-Pm was loaded in the second syringe, and time traces of fluorescence increase for the reverse reactions were recorded until displacement was >90% complete, ranging from 15 to 200 s. Final concentrations in the cell at the dead time of mixing were: [5F]FFR-[Lys]Pg, 10–20 nM; SK or SKΔK414, 59–2,000 nM; and FFR-Pm, 100–2,000 nM. Background scattering was subtracted, and F_o values of free [5F]FFR-[Lys]Pg were established, *i.e.* the signal at 100% displacement. Fluorescence quenches of the preformed SK·[5F]FFR-[Lys]Pg complexes in the dead time (4 ms) of the mixing step with FFR-Pm were compared for consistency with the values for forward reactions of SK and [5F]FFR-[Lys]Pg under identical conditions. Unlike the SK reactions with labeled Pm, the reactions with Pg were not stoichiometric due to weaker SK binding, and a range of SK and FFR-Pm concentrations was used to obtain time traces at various degrees of SK saturation with labeled [Lys]Pg and FFR-Pm. The faster and much larger displacement signal for FFR-Pm compared with FFR-Pg and the vastly lower scattering background of the SK·FFR-Pm complex were major reasons for performing displacement experiments with FFR-Pm rather than with FFR-Pg. The time traces were fit by a double exponential function (analogous to Equation 1) to obtain the observed first-order rate constants $k_{disp\,1}$ and $k_{disp\,2}$ for the fast and slow displacement processes.

Equilibrium Binding of [5F]FFR-Pg to SK and SKΔK414 in the Presence of Benzamidine—[5F]FFR-Pg (10 nM) was titrated with SK or SKΔK414 at 25 °C in 50 mM HEPES, 0.075 M NaCl, 1 mM EDTA, 1 mg/ml PEG 8000 buffer, pH 7.4 containing 50 mM benzamidine, 1 mg/ml BSA, and 1 μM FFR-CH_2Cl. Fluorescence titrations were performed with a Photon Technology International, Inc. fluorometer at excitation and emission wavelengths of 500 and 516 nm, respectively, with 2/8-nm excitation/emission band passes. Fluorescence changes were measured after equilibration for 5–10 min. Measurements were corrected for background (≤10%) by subtraction of blanks lacking [5F]FFR-Pg. Data were analyzed by the quadratic equation for binding of a single ligand (55). This analysis gave the dissociation constant (K_D) for binding of SK or SKΔK414 to [5F]FFR-Pg and the maximum fluorescence intensity change ($\Delta F_{max}/F_o$) with a stoichiometric factor (n) of 1 for binding of SK or SKΔK414 to labeled Pg.

Two-exponential time traces of forward and reverse reactions, SK dependences of $k_{obs\,1,2}$, and equilibrium binding of SK and SKΔK414 to [5F]FFR-Pg in benzamidine buffer were analyzed by nonlinear least square fitting with SCIENTIST Software (MicroMath). All reported estimates of error represent ±2 S.D.

Numerical Integration Analysis of the Forward and Reverse Reactions—Arrays of progress curves for SK·[5F]FFR-Pg formation and displacement of labeled Pg from the complex were analyzed globally with the numerical integration program KinTek Explorer 3.0 (67–69) for each set of reactants, concentration ranges, and buffer conditions. Five arrays were performed in the absence of lysine analogs: fluorescence amplitude changes of [5F]FFR-[Lys]Pg binding to nSK, WT-SK, and SKΔK414; fluorescence amplitude changes of [5F]FFR-[Glu]Pg binding to nSK; and anisotropy changes of [5F]FFR-[Lys]Pg binding to nSK. Three arrays were performed in 6-AHA: fluorescence amplitude changes of [5F]FFR-[Lys]Pg binding to nSK and SKΔK414 and [5F]FFR-[Glu]Pg binding to nSK. Two arrays were performed in benzamidine: fluorescence amplitude changes of [5F]FFR-[Lys]Pg binding to nSK and SKΔK414.

$$\mathrm{SK} + \mathrm{Pg} \underset{}{\overset{K_1}{\rightleftharpoons}} \mathrm{SK{\cdot}Pg\ 1} \underset{k_{-2}}{\overset{k_2}{\rightleftharpoons}} \mathrm{SK{\cdot}Pg\ 2} \underset{k_{-3}}{\overset{k_3}{\rightleftharpoons}} \mathrm{SK{\cdot}Pg\ 3}$$

SCHEME 1

$$\mathrm{SK} + \mathrm{Pm} \underset{}{\overset{K_4}{\rightleftharpoons}} \mathrm{SK{\cdot}Pm\ 1} \underset{k_{-5}}{\overset{k_5}{\rightleftharpoons}} \mathrm{SK{\cdot}Pm\ 2} \underset{k_{-6}}{\overset{k_6}{\rightleftharpoons}} \mathrm{SK{\cdot}Pm\ 3}$$

SCHEME 2

The mechanism included Scheme 1 for three-step SK·[5F]FFR-Pg binding and Scheme 2 for competitive three-step SK·FFR-Pm binding. The dissociation constants K_1 and K_4 for formation of the SK·Pg 1 and SK·Pm 1 encounter complexes represent the ratios k_{-1}/k_1 and k_{-4}/k_4 where k_1 and k_4 are the second-order association rate constants and k_{-1} and k_{-4} are the first-order rate constants for dissociation of the encounter complex. K_1, k_2, k_{-2}, k_3, and k_{-3} in this mechanism are equivalent to K_1, $k_{\mathrm{lim}\,1}$, $k_{\mathrm{off}\,1}$, $k_{\mathrm{lim}\,2}$, and $k_{\mathrm{off}\,2}$, respectively, in Equation 2. The three-step mechanism for SK·Pm stabilization was validated in a previous study (59).

Time traces of fluorescence quenches were transformed to increases by plotting $\Delta F/F_o$ expressed as functions of the formation and stabilization of SK·Pg 1, SK·Pg 2, and SK·Pg 3 complexes using positive amplitude factors as KinTek Explorer does not accept negative parameters. The set of fluorescence anisotropy increases was analyzed without transformation. The fractional change in fluorescence intensity or anisotropy was expressed as $\Delta F/F_o = f_2 \times ([\mathrm{SK{\cdot}Pg\ 2}]/[\mathrm{Pg}]_o) + f_3 \times ([\mathrm{SK{\cdot}Pg\ 3}]/[\mathrm{Pg}]_o)$ where $[\mathrm{Pg}]_o$ is the total [5F]FFR-Pg concentration, which is equal to the sum of $\mathrm{Pg}_{\mathrm{free}}$, SK·Pg 1, SK·Pg 2, and SK·Pg 3; [SK·Pg 2] and [SK·Pg 3] are the concentrations of these complexes at time t; and f_2 and f_3 the respective fractional amplitude factors for these complexes. The SK·Pg 1 complex does not contribute to fluorescence change. This expression allowed simultaneous analysis of time traces with different [5F]FFR-Pg concentrations.

Fitting Strategy—The on-rate constant k_1 for formation of the encounter complex was initially constrained at $1 \times 10^8\ \mathrm{M}^{-1}\ \mathrm{s}^{-1}$ as determined experimentally for SK binding to unlabeled [Lys]Pg (7), and the assumption was made that similar on-rates would apply for reactions of SK with [5F]FFR-[Lys]Pg and [5F]FFR-[Glu]Pg and of SKΔK414 with [5F]FFR-[Lys]Pg in all of our experimental buffers. Upon refinement of the other parameters, fitting k_1 yielded values that were close to $1 \times 10^8\ \mathrm{M}^{-1}\ \mathrm{s}^{-1}$ under all these conditions, justifying our choice of this value as an initial estimate. The parameters K_1, k_2, k_{-2}, k_3, and k_{-3} were initially constrained to K_1, $k_{\mathrm{lim}\,1}$, $k_{\mathrm{off}\,1}$, $k_{\mathrm{lim}\,2}$, and $k_{\mathrm{off}\,2}$ obtained from the SK dependences (Table 1, superscript b), and refinement of these initial estimates ultimately provided the final fits (superscripts a and aa).

Analysis of [5F]FFR-[Lys]Pg displacement required known concentrations of free Pg and the intermediates SK·Pg 1, SK·Pg 2, and SK·Pg 3 present at the start of the reaction with FFR-Pm as there was substantial partitioning among these species at equilibration of the SK·[5F]FFR-[Lys]Pg complex. They were calculated iteratively using the starting concentrations of SK and [5F]FFR-[Lys]Pg used to form the complex, the forward and reverse rate constants, and the known dissociation constant for the competitive, unlabeled SK·FFR-Pm complex. The sum of the calculated free Pg, SK·Pg 1, SK·Pg 2, and SK·Pg 3 concentrations was in agreement with the total Pg concentration, indicating that mass balance was conserved during the fits. Complexes of SK with labeled and unlabeled Pm have indistinguishable affinities in the absence of lysine analogs (26, 48) and in 6-AHA (26, 27), suggesting that the binding parameters for SK are very similar for labeled and unlabeled FFR-Pm. This allowed fixing K_4, k_5, k_{-5}, k_6, and k_{-6} to our previously determined values for [5F]FFR-Pm binding in each buffer system (59). Displacement of [5F]FFR-[Lys]Pg binding to SK and SKΔK414 in benzamidine was analyzed with fitted K_D values of 227 ± 11 and 200 ± 20 pM for FFR-Pm binding, respectively, in agreement with the previously determined 130 and 250 pM (59).

The large scattering background introduced variable uncertainty in the amplitude factors f_2 and f_3 for [SK·Pg 2] and [SK·Pg 3] at increasing SK concentrations, resulting in non-random residuals when imposing global f_2 and f_3 fits on the complete data sets. Initial estimates of the rate constants obtained by global fitting of f_2 and f_3 were fixed, and individual f_2 and f_3 amplitude factors were assigned as fitted parameters for time traces at each SK concentration. This largely eliminated the non-random deviations. Subsequent fixing of all the individual amplitude parameters provided further refinement of the fitted rate constants with only subtle differences from the original estimates.

The overall K_D values for the final, stabilized complexes were calculated from Equation 3 using the rate constants obtained by numerical analysis and compared with $K_{D,\,\mathrm{overall}}$ obtained independently from equilibrium binding.

$$K_{D,\,\mathrm{overall}} = \frac{[\mathrm{SK}][\mathrm{Pg}]}{[\mathrm{SK{\cdot}Pg\ 1}] + [\mathrm{SK{\cdot}Pg\ 2}] + [\mathrm{SK{\cdot}Pg\ 3}]} = \frac{K_1K_2K_3}{1 + K_2K_3 + K_3} \qquad \text{(Eq. 3)}$$

RESULTS

Stopped-flow Kinetics of SK Binding to [5F]FFR-[Lys]Pg—Time traces of fractional quenches of fluorescence intensity ($\Delta F/F_o$) and increases of anisotropy ($\Delta r/r_o$) following rapid mix-

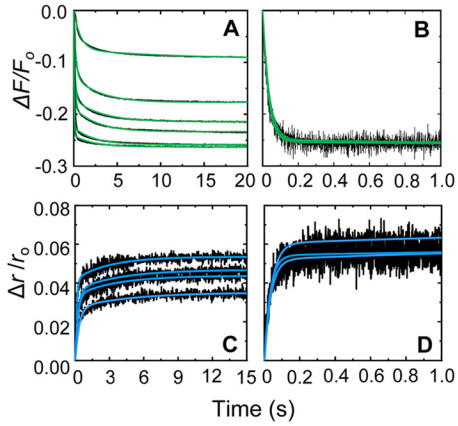

FIGURE 1. **Stopped-flow fluorescence changes of SK binding to [5F]FFR-[Lys]Pg.** *A* and *B*, the fractional fluorescence intensity changes ($\Delta F/F_o$) following rapid mixing of [5F]FFR-[Lys]Pg and nSK *versus* time are shown in the absence of lysine analogs at 20 nM [5F]FFR-[Lys]Pg and 0.42, 0.84, 1.58, 3.00, and 5.00 μM nSK (*A*) and at 10 nM [5F]FFR-[Lys]Pg and 8.2, 11.7, and 17.6 μM nSK (*B*). *C* and *D*, fractional fluorescence anisotropy changes ($\Delta r/r_o$) are shown for 20 nM [5F]FFR-[Lys]Pg and 0.075, 0.15, 0.20, and 0.52 μM nSK (*C*) and for 4.7, 7.0, and 14 μM nSK (*D*). *Green* and *blue solid lines* represent the fits from numerical integration with the parameters given in Table 1 as described under "Experimental Procedures."

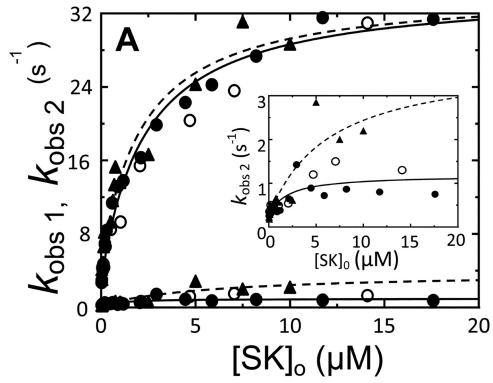

FIGURE 2. **SK concentration dependence of the kinetics of [5F]FFR-[Lys]Pg binding in the absence of lysine analogs.** Dependences of $k_{obs\,1}$ and $k_{obs\,2}$ (●, nSK, fluorescence intensity; ○, nSK, fluorescence anisotropy; ▲, WT-SK, fluorescence intensity) on $[SK]_o$ are shown for binding to 10–20 nM [5F]FFR-[Lys]Pg. The *inset* shows the $k_{obs\,2}$ dependence on an enlarged scale. *Solid* and *dashed lines* represent the least square fits by Equation 2 with the parameters given in Table 1 for the reactions with nSK and WT-SK, respectively.

ing of [5F]FFR-Pg with excess SK in the absence of lysine analogs were distinctly biexponential with first-order rate constants $k_{obs\,1}$ and $k_{obs\,2}$ fitted by Equation 1. Time traces started at zero $\Delta F/F_o$ with F at 4 ms $\approx F_o$ of a control reaction with only [5F]FFR-Pg, indicating no significant fluorescence change associated with encounter complex formation. Representative changes in fluorescence intensity and anisotropy of [5F]FFR-[Lys]Pg binding to nSK are shown in Fig. 1. Colored lines represent global fits of forward and reverse reactions by numerical analysis. The first-order rate constants $k_{obs\,1}$ and $k_{obs\,2}$ for the fast and slow fluorescence changes obtained from the individual biexponential fits increased hyperbolically with increasing SK concentration. Fig. 2 shows the nSK and WT-SK dependences in the absence of effectors. The hyperbolic dependences of $k_{obs\,1}$ and the much smaller $k_{obs\,2}$, respectively, indicated saturation of the encounter complex and the subsequent conformational intermediate (Fig. 2, *inset*). The parameters K_1, $k_{lim\,1}$, $k_{lim\,2}$, $k_{off\,1}$, and $k_{off\,2}$ obtained by fitting the binding rate constants by Equation 2 are given in Table 1 (superscript b). The reverse rate constants $k_{off\,1}$ and $k_{off\,2}$ for the two conformational steps given by the extrapolated intercepts of $k_{obs\,1}$ and $k_{obs\,2}$ at zero SK were 4.0 ± 1.0 and 0.25 ± 0.10 s^{-1}. The dissociation constants K_1 for the encounter complexes of [5F]FFR-[Lys]Pg with nSK and WT-SK were 3.4 ± 1.0 and 2.1 ± 1.2 μM.

Stopped-flow Kinetics of SKΔK414 Binding to [5F]FFR-[Lys]Pg—Progress curves of SKΔK414 binding to [5F]FFR-[Lys]Pg and the SKΔK414 dependence of $k_{obs\,1}$ and $k_{obs\,2}$ are shown in Fig. 3 with colored lines representing the global fits of the forward and reverse reactions by numerical analysis. The SKΔK414 mutant bound ~6-fold more weakly than nSK with a K_1 of 19 ± 4 μM (Table 1, superscript b), suggesting that the COOH-terminal SK Lys^{414} increases the efficiency of initial docking of SK with Pg by interacting with a kringle.

Effects of 6-AHA on the Kinetics of SK and SKΔK414 Binding to [5F]FFR-[Lys]Pg—Time traces of the forward reactions and the SK dependences of k_{obs1} and k_{obs2} in 50 mM 6-AHA are shown in Fig. 4. Blocking the LBSs on kringles K1, K4, and K5 with 6-AHA decreased the affinity of the encounter complex to a K_1 value of 7 μM (Table 1, superscript b), which is comparable with that of SKΔK414 binding in the absence of 6-AHA. The SK and SKΔK414 dependences of these weak binding interactions were not saturable, preventing accurate determination of K_1; hence values ranging from 7 to 20 μM may be considered comparable. A weak encounter complex with a K_1 value of 14 μM was also observed for SKΔK414 binding in 6-AHA (Fig. 5). The limiting rate constants $k_{lim\,1}$ and $k_{lim\,2}$ and the off-rates $k_{off\,1}$ and $k_{off\,2}$ determining the conformational changes following encounter complex formation were similar for SK and SKΔK414 binding to [5F]FFR-[Lys]Pg in the absence and presence of 6-AHA. Total amplitudes of the time traces fit by Equation 1 reflected overall maximal fluorescence changes ($\Delta F_{max}/F_o$) for SK and SKΔK414 binding to [5F]FFR-Pg in agreement with equilibrium binding results in the absence and presence of 6-AHA (27, 48).

Effects of Benzamidine on the Kinetics of SK and SKΔK414 Binding to [5F]FFR-[Lys]Pg—Blocking kringles K1, K2, and K5 with 50 mM benzamidine weakened the K_1 of the [5F]FFR-[Lys]Pg encounter complex with SK to 12 μM (Table 1, superscript b). Time traces of the forward reactions of SK binding were not resolvable into two phases and appeared as single exponential curves, whereas SKΔK414 binding was clearly biphasic. Progress curves for binding of SK and SKΔK414 and their concentration dependences of $k_{obs\,1}$ and $k_{obs\,2}$ in benzamidine are shown in Fig. 6. The limiting rate $k_{lim\,1}$ in benzamidine was ~5-fold faster for SK binding and ~2.3-fold faster for SKΔK414 binding compared with the values in 6-AHA and in the absence of lysine analogs (Table 1, superscript b). The ~30% lower maximal fluorescence changes than those for equilibrium binding in the presence of benzamidine described below (Table 1) may be due to the scattering properties of Pg complexes in benzamidine being differentially affected by the optical cell geometry and path length of the Photon Technology International, Inc. fluorometer and the stopped-flow instrument.

TABLE 1

Kinetic and equilibrium binding parameters for the formation of SK·Pg and SKΔK414·Pg complexes

Kinetic constants obtained from simultaneous numerical integration of the forward and reverse reactions[a], forward reactions measured as anisotropy changes[aa], and SK dependences of the fast and slow phases of the forward reactions[b] are listed for reaction Scheme 1 in the absence of kringle ligands (no effector) and in the presence of saturating 6-AHA or benzamidine. $K_{D,\,overall}$ was calculated from the individual kinetic parameters[c] and measured by fluorescence titration[d]. For analysis of near-linear SK dependences K_1 was fixed to the value obtained by numerical analysis[fixed]. Amplitudes of change in fluorescence intensity ($\Delta F_{max}/F_o$) were from numerical analysis (f_2 and f_3 for SK·Pg 2 and SK·Pg 3, respectively) and equilibrium binding (overall value). Reported errors are 2 × S.D. and were calculated by error propagation for compound parameters.

	$K_{1\,(encounter)}$	k_2 ($\approx k_{lim\,1}$)	k_{-2} ($\approx k_{off\,1}$)	k_3 ($\approx k_{lim\,2}$)	k_{-3} ($\approx k_{off\,2}$)	$K_{D,\,overall}$	$\Delta F_{max}/F_o$
	μM	s^{-1}	s^{-1}	s^{-1}	s^{-1}	μM	%
[5F]FFR-[Lys]Pg, no effector							
nSK	2.8 ± 0.3[a]	34 ± 2[a]	3.5 ± 0.4[a]	0.34 ± 0.04[a]	0.15 ± 0.01[a]	0.086 ± 0.018[a,c]	−30 ± 9[a], −25 ± 6[a]
	1.8 ± 0.2[aa]	33 ± 2[aa]	1.8 ± 0.1[aa]	0.26 ± 0.06[aa]	0.12 ± 0.02[aa]	0.030 ± 0.018[aa,c]	
	3.4 ± 1.0[b]	33 ± 3[b]	4.0 ± 1.0[b]	0.90 ± 0.30[b]	0.25 ± 0.10[b]	0.044 ± 0.009[d]	−28 ± 1[d]
WT-SK	0.94 ± 0.01[a]	27 ± 1[a]	3.5 ± 0.2[a]	0.44 ± 0.03[a]	0.22 ± 0.01[a]	0.039 ± 0.005[a,c]	−26 ± 8[a], −24 ± 4[a]
	2.1 ± 1.2[b]	30 ± 6[b]	4.5 ± 2.0[b]	3.60 ± 1.60[b]	0.24 ± 0.16[b]	0.028 ± 0.006[d]	−23 ± 1[d]
SKΔK414	20.3 ± 0.2[a]	31 ± 1[a]	2.5 ± 0.1[a]	0.17 ± 0.01[a]	0.20 ± 0.01[a]	0.84 ± 0.09[a,c]	−24 ± 4[a], −30 ± 5[a]
	19.0 ± 4.0[b]	25 ± 4[b]	2.3 ± 0.6[b]	0.10 ± 0.08[b]	0.30 ± 0.06[b]	0.60 ± 0.20[d]	−24 ± 2[d]
6-AHA							
nSK	10.5 ± 0.7[a]	28 ± 3[a]	3.7 ± 0.2[a]	0.10 ± 0.02[a]	0.23 ± 0.01[a]	0.89 ± 0.20[a,c]	−22 ± 8[a], −37 ± 8[a]
	7.0 ± 5.0[b]	25 ± 8[b]	2.0 ± 1.0[b]	2.00 ± 2.00[b]	0.19 ± 0.09[b]	0.56 ± 0.09[d]	−23 ± 1[d]
SKΔK414	16.3 ± 0.6[a]	31 ± 2[a]	2.7 ± 0.1[a]	0.19 ± 0.02[a]	0.16 ± 0.01[a]	0.64 ± 0.10[a,c]	−23 ± 6[a], −29 ± 3[a]
	14.0 ± 2.0[b]	31 ± 3[b]	1.0 ± 0.6[b]	0.15 ± 0.18[b]	0.23 ± 0.02[b]	0.75 ± 0.35[d]	−24 ± 3[d]
Benzamidine							
nSK	11.4 ± 0.3[a]	156 ± 3[a]	3.2 ± 0.1[a]	0.07 ± 0.01[a]	0.15 ± 0.02[a]	0.16 ± 0.04[a,c]	−18 ± 7[a], −17 ± 8[a]
	12.0 ± 2.0[b]	150 ± 15[b]	2.0 ± 1.0[b]			0.20 ± 0.02[d]	−30 ± 1[d]
SKΔK414	16.0 ± 0.3[a]	69 ± 4[a]	4.8 ± 0.2[a]	0.26 ± 0.02[a]	0.24 ± 0.02[a]	0.52 ± 0.06[a,c]	−27 ± 7[a], −23 ± 3[a]
	16.0 ± 10.0[b]	70 ± 30[b]	4.0 ± 2.0[b]	1.30 ± 0.40[b]	0.27 ± 0.10[b]	0.80 ± 0.10[d]	−38 ± 1[d]
[5F]FFR-[Glu]Pg, no effector							
nSK	18.1 ± 0.2[a]	42 ± 1[a]	2.8 ± 0.1[a]	0.10 ± 0.01[a]	0.19 ± 0.01[a]	0.76 ± 0.20[a,c]	−31 ± 3[a], −25 ± 4[a]
	18.1[b,fixed]	46 ± 5[b]	2.0 ± 0.5[b]	1.00 ± 0.20[b]	0.17 ± 0.02[b]	0.58 ± 0.08[d]	−32 ± 1[d]
6-AHA							
nSK	15.4 ± 0.2[a]	30 ± 1[a]	3.2 ± 0.1[a]	0.35 ± 0.01[a]	0.19 ± 0.01[a]	0.56 ± 0.08[a,c]	−18 ± 8[a], −16 ± 7[a]
	15.4[b,fixed]	36 ± 5[b]	1.8 ± 0.6[b]	2.94 ± 0.21[b]	0.12 ± 0.03[b]	0.60 ± 0.07[d]	−23 ± 1[d]

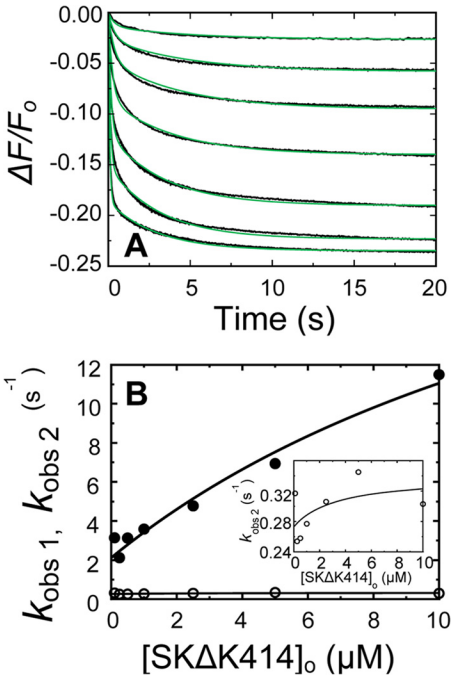

FIGURE 3. **Kinetics of SKΔK414 binding to [5F]FFR-[Lys]Pg in the absence of lysine analogs.** *A*, the fractional fluorescence intensity changes ($\Delta F/F_o$) following rapid mixing of [5F]FFR-[Lys]Pg and SKΔK414 *versus* time are shown in the absence of lysine analogs at 20 nM [5F]FFR-[Lys]Pg and 0.1, 0.25, 0.5, 1.0, 2.5, 5.0, and 10 μM SKΔK414. *Green solid lines* represent the fits from numerical integration as described under "Experimental Procedures." *B*, dependences of $k_{obs\,1}$ and $k_{obs\,2}$ (● and ○) on the total SKΔK414 concentration (*[SKΔK414]$_o$*) are shown for binding to 20 nM [5F]FFR-[Lys]Pg. The *inset* shows the $k_{obs\,2}$ dependence on an enlarged scale. *Solid lines* represent the fits by Equation 2 with the parameters given in Table 1. Experiments were performed and analyzed as described under "Experimental Procedures."

Stopped-flow Kinetics of SK Binding to [5F]FFR-[Glu]Pg—Biexponential binding of SK to [5F]FFR-[Glu]Pg was not saturable, and the k_2/K_1 ratios in the absence and presence of 6-AHA were indistinguishable and similar to those for [5F]FFR-[Lys]Pg binding to SKΔK414 in the absence of kringle ligands and to nSK and SKΔK414 binding in 6-AHA (Fig. 7). Fitting of these near linear dependences was performed using fixed, lower limit K_1 values that were reasonably resolvable by numerical integration (see below). The limiting rate constants $k_{lim\,1}$ and $k_{lim\,2}$ and the off-rates $k_{off\,1}$ and $k_{off\,2}$ were similar to those for SK and SKΔK414 binding to [5F]FFR-[Lys]Pg in the absence of lysine analogs and in 6-AHA (Table 1, superscript b).

Competitive Displacement of [5F]FFR-[Lys]Pg from Its Complex with nSK, WT-SK, and SKΔK414 by FFR-Pm—Mixing a ~5–100-fold excess of unlabeled FFR-Pm with the preformed complexes of SK and SKΔK414 with [5F]FFR-[Lys]Pg at varying degrees of saturation caused a rapid, biexponential increase of fluorescence, approaching the initial fluorescence intensity. Analysis of the time traces by Equation 1 yielded perfect fits with random residuals (not shown) and gave $k_{disp\,1}$ and $k_{disp\,2}$ values for the fast and slow exponential phases of the displacement reactions. Representative averaged traces for SK and SKΔK414 displacement by FFR-Pm are shown in Figs. 8 and 9 with the colored lines representing global fits of forward and reverse reactions by numerical analysis. These processes represent rapid reversal of [5F]FFR-[Lys]Pg binding to SK and SKΔK414 and parallel formation of non-fluorescent complexes with FFR-Pm. Saturation of Pg required high SK and SKΔK414 concentrations and consequently high FFR-Pm to bind free SK and SKΔK414 and to displace labeled Pg from the complexes. Therefore we expressed $k_{disp\,1}$ and $k_{disp\,2}$ as dependences of free

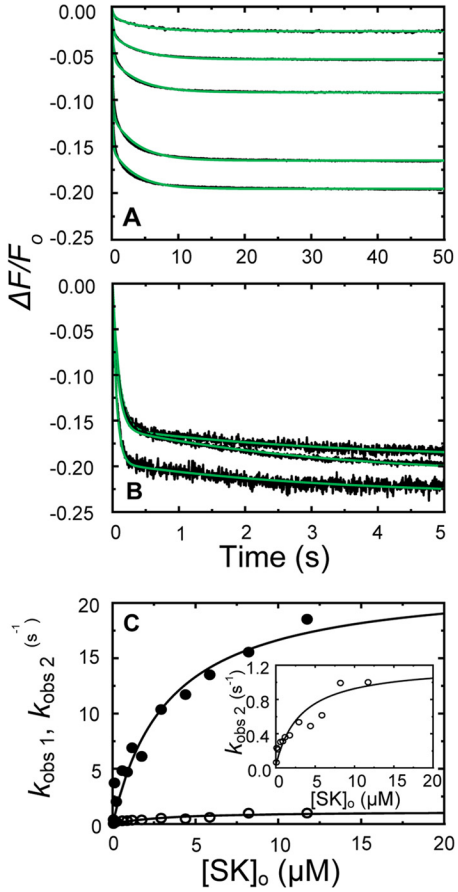

FIGURE 4. **Kinetics of SK binding to [5F]FFR-[Lys]Pg in 50 mM 6-AHA.** *A* and *B*, the fractional fluorescence intensity changes ($\Delta F/F_o$) following rapid mixing of [5F]FFR-[Lys]Pg and nSK *versus* time in 50 mM 6-AHA are shown for 20 nM [5F]FFR-[Lys]Pg and 0.10, 0.26, 0.53, 1.53, and 3.06 μM nSK (*A*) and at 10 nM [5F]FFR-[Lys]Pg and 2.93, 4.40, and 8.21 μM nSK (*B*). *Green solid lines* represent the fits from numerical integration as described under "Experimental Procedures." *C*, dependences of $k_{obs\ 1}$ (●) and $k_{obs\ 2}$ (○) on the total nSK concentration ($[SK]_o$) are shown for binding to 10–20 nM [5F]FFR-[Lys]Pg. The *inset* shows the $k_{obs\ 2}$ dependence on an enlarged scale. *Solid lines* represent the least-squares fits by Equation 2 with the parameters given in Table 1. Experiments were performed and analyzed as described under "Experimental Procedures."

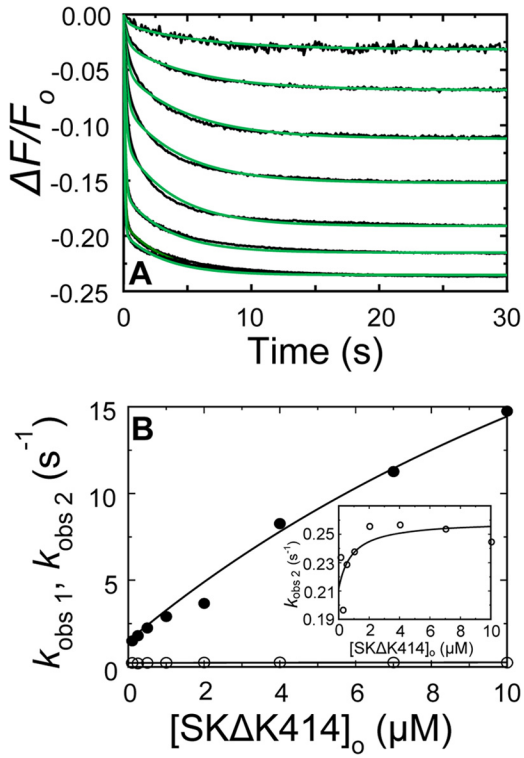

FIGURE 5. **Kinetics of SKΔK414 binding to [5F]FFR-[Lys]Pg in 50 mM 6-AHA.** *A*, the fractional fluorescence intensity changes ($\Delta F/F_o$) following rapid mixing of [5F]FFR-[Lys]Pg and SKΔK414 *versus* time in 50 mM 6-AHA are shown for 20 nM [5F]FFR-[Lys]Pg and 0.1, 0.25, 0.5, 1, 2, 4, 7, and 10 μM SKΔK414. *Green solid lines* represent the fits from numerical integration as described under "Experimental Procedures." *B*, dependences of $k_{obs\ 1}$ (●) and $k_{obs\ 2}$ (○) on the total SKΔK414 concentration ($[SK\Delta K414]_o$) are shown for binding to 20 nM [5F]FFR-[Lys]Pg. The *inset* shows the $k_{obs\ 2}$ dependence on an enlarged scale. *Solid lines* represent the least square fits by Equation 2 with the parameters given in Table 1. Experiments were performed and analyzed as described under "Experimental Procedures."

rather than total FFR-Pm calculated by numerical integration. The rates were independent of free FFR-Pm, consistent with extremely tight binding of SK and SKΔK414 to plasmin (59), and were similar for [Lys]Pg and [Glu]Pg in the absence and presence of lysine analogs. The off-rate for the fast process, $k_{disp\ 1}$, was 0.90 ± 0.60 s^{-1}, which is modestly lower than the averaged $k_{off\ 1}$ of 2.60 ± 1.2 s^{-1} determined from the SK dependences of the forward reactions and the equivalent averaged k_{-2} of 3.2 ± 1.6 s^{-1} from numerical analysis (see below). The $k_{disp\ 2}$ off-rate for the slow phase was 0.13 ± 0.09 s^{-1}, which is similar to the averaged $k_{off\ 2}$ of 0.22 ± 0.12 s^{-1} from the SK dependences and the equivalent averaged k_{-3} of 0.19 ± 0.08 s^{-1} from numerical analysis.

Equilibrium Binding of [5F]FFR-[Lys]Pg to SK and SKΔK414 in the Presence of 50 mM Benzamidine—We determined the affinity and fluorescence change for SK and SKΔK414 equilibrium binding to [5F]FFR-[Lys]Pg in 50 mM benzamidine to characterize the effect of this K1, K2, and K5 ligand on the overall equilibrium binding constant $K_{D,\ overall}$ and to compare this affinity with $K_{D,\ overall}$ calculated from the forward and reverse constants obtained by the binding kinetics (Fig. 10). Analysis of the titrations indicated that SK bound with a K_D of 200 ± 20 nM and $\Delta F_{max}/F_o$ of −30 ± 1%. The affinity was ~5-fold weaker than in the absence of kringle ligands but still ~3-fold tighter than in 6-AHA. SKΔK414 bound labeled [Lys]Pg with a $\Delta F_{max}/F_o$ of −38 ± 1% and K_D of 800 ± 100 nM. This affinity was similar to that of SK in 6-AHA, SKΔK414 with and without 6-AHA (48), and SK binding to [5F]FFR-[Glu]Pg with and without 6-AHA (27, 48).

Numerical Integration Analysis of the Forward and Reverse Reactions—Fitted values for K_1, the rate constants for both conformational steps, and the fluorescence amplitudes were in good agreement with those obtained from two-exponential analysis and equilibrium binding and are given in Table 1 (superscript a, fluorescence intensity, and superscript aa, fluorescence anisotropy). The results indicated that formation of fluorescently silent SK·Pg 1 occurs in the dead time of the reaction and that subsequent partitioning occurs between SK·Pg 2 and SK·Pg 3.

The SK·[5F]FFR-[Lys]Pg encounter complex was weakened ~10–20-fold by blocking LBSs on the Pg kringles and by loss of Lys^{414}. The rate constant k_2 for the first conformational step ranged from 25 to 45 s^{-1} in the absence and presence of 6-AHA

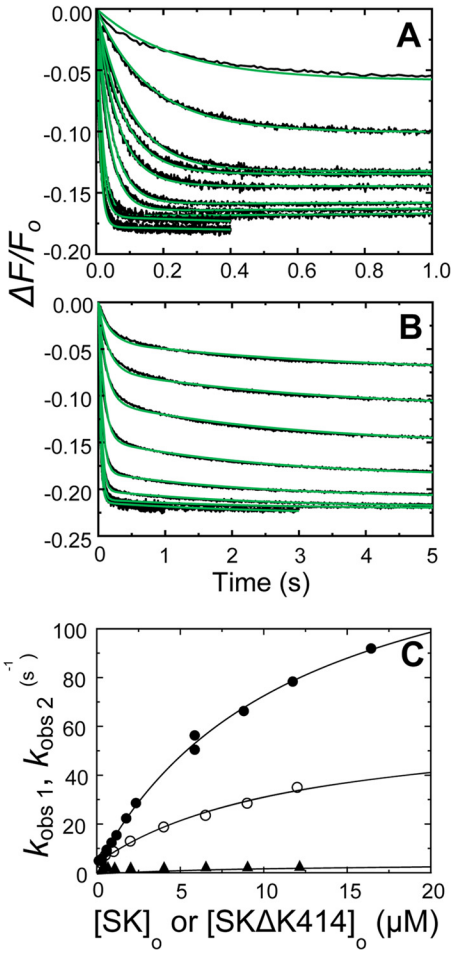

FIGURE 6. **Kinetics of SK and SKΔK414 binding to [5F]FFR-[Lys]Pg in 50 mM benzamidine.** *A*, the fractional fluorescence intensity changes ($\Delta F/F_o$) following rapid mixing of [5F]FFR-[Lys]Pg and nSK *versus* time in 50 mM benzamidine are shown for 10 or 15 nM [5F]FFR-[Lys]Pg and 0.12, 0.29, 0.59, 0.88, 1.17, 1.76, 2.34, 5.86, 8.8, 11.73, and 16.42 μM nSK. *B*. the fractional fluorescence intensity changes ($\Delta F/F_o$) following rapid mixing of [5F]FFR-[Lys]Pg and SKΔK414 *versus* time in 50 mM benzamidine are shown for 20 nM [5F]FFR-[Lys]Pg and 0.25, 1, 2, 4, 6.5, 9, and 12 μM SKΔK414. *Green solid lines* represent the fits from numerical integration as described under "Experimental Procedures." *C*, dependences of k_{obs1} (●) on the total nSK concentration ($[SK]_o$) and $k_{obs\,1}$ and $k_{obs\,2}$ (○ and ▲) on the total SKΔK414 concentration ($[SK\Delta K414]_o$) are shown for binding to 10–20 nM [5F]FFR-[Lys]Pg. *Solid lines* represent the least square fits by Equation 2 with the parameters given in Table 1. Experiments were performed and analyzed as described under "Experimental Procedures."

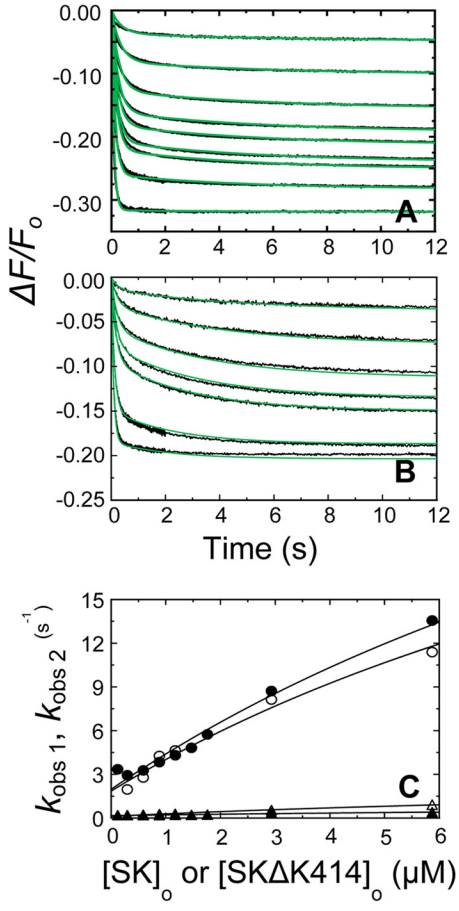

FIGURE 7. **Kinetics of SK binding in the [5F]FFR-[Glu]Pg complex in the absence of lysine analogs and at saturating 6-AHA.** *A*, the fractional fluorescence intensity changes ($\Delta F/F_o$) following rapid mixing of [5F]FFR-[Glu]Pg and nSK *versus* time in the absence of lysine analogs are shown for 13 or 20 nM [5F]FFR-[Glu]Pg and 0.12, 0.29, 0.59, 0.88, 1.17, 1.47, 1,76, 2.93, and 5.87 μM nSK. *B*, the fractional fluorescence intensity changes ($\Delta F/F_o$) following rapid mixing of [5F]FFR-[Glu]Pg and nSK *versus* time in 50 mM 6-AHA are shown for 13 or 20 nM [5F]FFR-[Glu]Pg and 0.12, 0.29, 0.59, 0.88, 1.17, 2.93, and 5.87 μM nSK. *Green solid lines* represent the fits from numerical integration as described under "Experimental Procedures." *C*, dependences of $k_{obs\,1}$ (● and ○) and $k_{obs\,2}$ (▲ and △) on the total nSK concentration ($[SK]_o$) are shown for binding to 10–20 nM [5F]FFR-[Glu]Pg in the absence of lysine analogs (*filled symbols*) and in 50 mM 6-AHA (*open symbols*). *Solid lines* represent the least square fits by Equation 2 with the parameters given in Table 1. Experiments were performed and analyzed as described under "Experimental Procedures."

but increased substantially in benzamidine, suggesting a decrease in conformational restraint.

The rate constants k_{-2} and k_{-3} for the reverse reactions were equivalent to $k_{off\,1}$ and $k_{off\,2}$ from hyperbolic fitting of the SK dependences of the forward reaction rates and to $k_{disp\,1}$ and $k_{disp\,2}$ for the biexponential appearance of free [5F]FFR-[Lys]Pg in competitive displacement by FFR-Pm. The analytical solution of the overall k_{off} value for a three-step reaction is only straightforward under conditions of single exponential kinetics (70); however, the agreement of $k_{off\,2}$ and $k_{disp\,2}$ with k_{-3} from numerical analysis suggests that dissociation is limited by k_{-3}. The off-rates were unaffected by lysine analogs.

In the absence of effectors, $K_{D,\,overall}$ for SK binding to [5F]FFR-[Lys]Pg ranged from 30 ± 18 to 86 ± 18 nM in agreement with the results from equilibrium binding (27, 48). Deletion of SK Lys^{414} or blocking the LBSs with 6-AHA caused an increase of $K_{D,\,overall}$ to 0.5–0.9 μM, which is identical to that for [Glu]Pg binding. In benzamidine, $K_{D,\,overall}$ for binding of intact SK to labeled [Lys]Pg was 0.2 μM, possibly reflecting the contribution of the large forward rate for the first tightening step.

Within global data sets, the errors in the amplitude factors f_2 for the fast conformational step and f_3 for the slow step were ~30 and ~18%, respectively (2 × S.D.). Numerical integration fits for the forward and reverse reactions are shown as colored lines in the figures.

DISCUSSION

The present study demonstrates a minimal three-step sequential mechanism for binding of SK to [5F]FFR-Pg, consisting of an encounter complex with affinity in the low micromolar range followed by at least two resolvable conformational

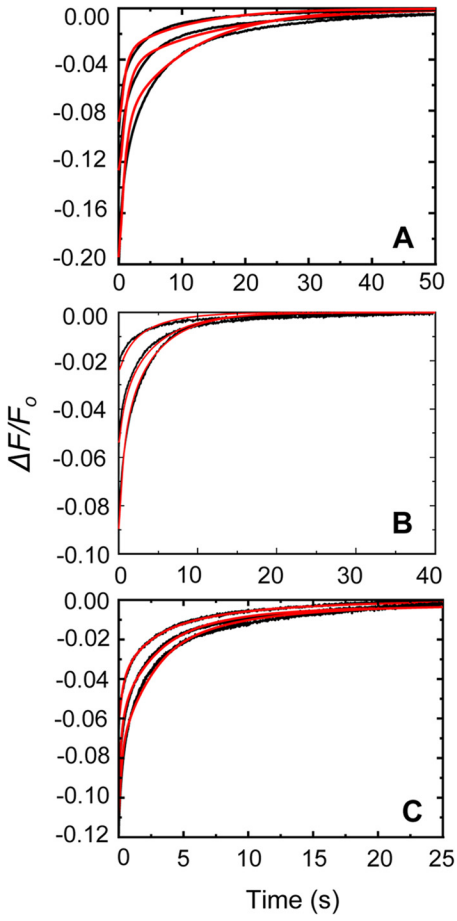

FIGURE 8. **Competitive dissociation of [5F]FFR-[Lys]Pg from its complex with nSK by FFR-Pm.** *A*, displacement of [5F]FFR-[Lys]Pg from its stabilized complex with nSK by FFR-Pm in the absence of lysine analogs is shown at dead time mixing concentrations of 20 nM [5F]FFR-[Lys]Pg, 0.06 μM nSK, and 0.1 μM FFR-Pm (*top*); 0.12 μM nSK and 0.2 μM FFR-Pm (*middle*); and 0.23 μM nSK and 0.4 μM FFR-Pm (*bottom*). *B*, displacement of [5F]FFR-[Lys]Pg from its stabilized complex with nSK by FFR-Pm in 50 mM 6-AHA is shown at dead time mixing concentrations of 20 nM [5F]FFR-[Lys]Pg, 0.1 μM nSK, and 0.2 μM FFR-Pm (*top*); 0.25 μM nSK and 0.3 μM FFR-Pm (*middle*); and 0.5 μM nSK and 0.6 μM FFR-Pm (*bottom*). *C*, displacement of [5F]FFR-[Lys]Pg from its stabilized complex by FFR-Pm in 50 mM benzamidine is shown at dead time mixing concentrations of 20 nM [5F]FFR-[Lys]Pg, 0.1 μM nSK, and 0.2 μM FFR-Pm (*top*); 0.25 μM nSK and 0.3 μM FFR-Pm (*middle*); and 0.5 μM nSK and 0.6 μM FFR-Pm (*bottom*). *Red solid lines* represent the fits from numerical integration as described under "Experimental Procedures."

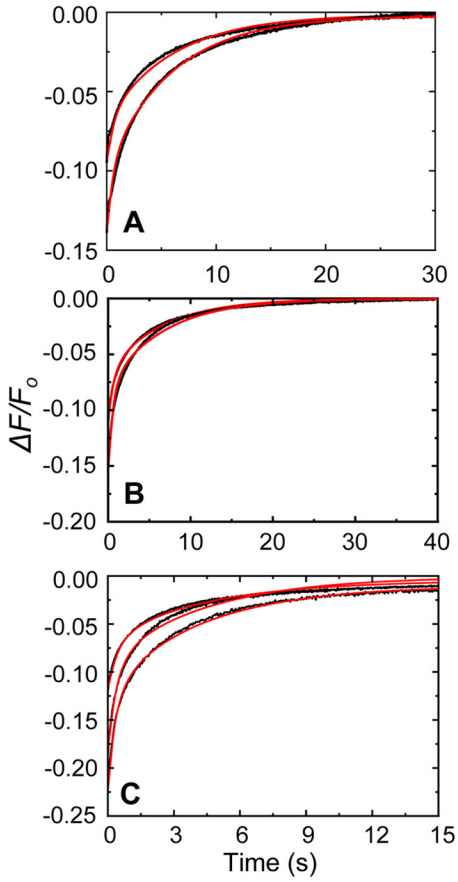

FIGURE 9. **Competitive dissociation of [5F]FFR-[Lys]Pg from its complex with SKΔK414 by FFR-Pm.** *A*. Displacement of [5F]FFR-[Lys]Pg from its stabilized complex with SKΔK414 by FFR-Pm in the absence of lysine analogs is shown at dead time mixing concentrations of 20 nM [5F]FFR-[Lys]Pg, 0.5 μM SKΔK414, and 0.5 μM FFR-Pm (*top*) and 1.0 μM SKΔK414 and 1.0 μM FFR-Pm (*bottom*). *B*, displacement of [5F]FFR-[Lys]Pg from its stabilized complex with SKΔK414 by FFR-Pm in 50 mM 6-AHA is shown at dead time mixing concentrations of 20 nM [5F]FFR-[Lys]Pg, 0.5 μM SKΔK414, and 0.7 μM FFR-Pm (*top*) and 1 μM SKΔK414 and 1.4 μM FFR-Pm (*bottom*). *C*, displacement of [5F]FFR-[Lys]Pg from its stabilized complex with SKΔK414 by FFR-Pm in 50 mM benzamidine is shown at dead time mixing concentrations of 20 nM [5F]FFR-[Lys]Pg, 0.5 μM SKΔK414, and 0.5 μM FFR-Pm (*top*); 1 μM SKΔK414 and 1.2 μM FFR-Pm (*middle*); and 2 μM SKΔK414 and 2 μM FFR-Pm (*bottom*). *Red solid lines* represent the fits from numerical integration as described under "Experimental Procedures."

steps (Fig. 11), which increase the affinity of the stabilized complex to ~30–86 nM. The first conformational step is the main tightening event, whereas the second step does not confer additional tightening. However, deletion of this second step in the mechanism resulted in single exponential curves that did not fit the data.

We previously discovered that a three-step mechanism also governs SK binding to labeled plasmin but with ~4,000-fold tighter $K_{D,\,\mathrm{overall}}$ values of 7–12 pM (59). The conformational changes caused a ~9,000-fold tightening of the Pm encounter complex but only a ~50-fold increase in affinity for Pg. We show here that substantial decreases in affinity of the encounter complex and the second conformational event are mainly responsible for the weaker SK binding to Pg in the stabilized complex.

The results suggest that the SK interactions with LBSs on [Lys]Pg are mainly limited to SK Lys^{414} binding to K4, whereas

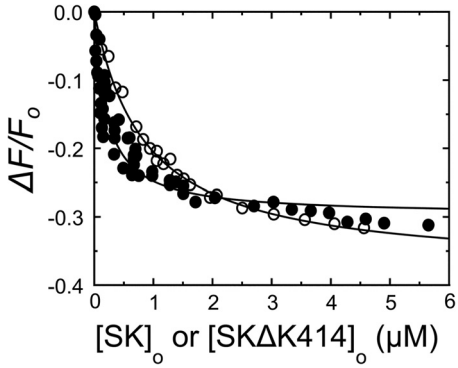

FIGURE 10. **Equilibrium binding of SK and SKΔK414 to [5F]FFR-[Lys]Pg in the presence of benzamidine.** The fractional change in fluorescence ($\Delta F/F_o$) of 20 nM [5F]FFR-[Lys]Pg in buffer containing 50 mM benzamidine is plotted as a function of the total nSK (●) or SKΔK414 (○) concentration ($[SK]_o$ or $[SK\Delta K414]_o$). *Solid lines* represent least square fits of the quadratic equation for binding of a single ligand with the parameters listed in the text and Table 1. Fluorescence titrations were performed and analyzed as described under "Experimental Procedures."

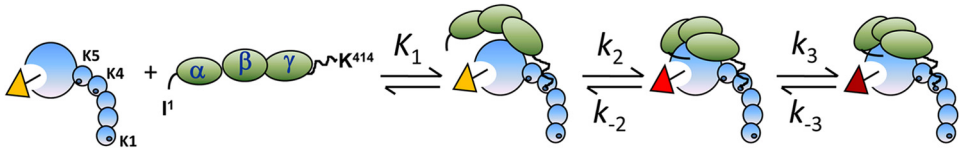

FIGURE 11. **The three-step mechanism of SK·[5F]FFR-[Lys]Pg catalytic complex formation.** [5F]FFR-[Lys]Pg is shown as *blue circles* in a hypothetical partially extended β-conformation. The five kringle domains are *small circles* with the LBSs of K1, K4, and K5 as *tiny black dimples*. The zymogen catalytic domain is the *larger blue circle* with the activated catalytic site in *white* locked into its conformation by the fluorescein probe (*ocher triangle*) covalently attached to the peptide chloromethyl ketone that has alkylated His^{57} (*black stem*). SK is shown by three *green ovals* representing the three β-grasp domains marked α, β, and γ. The NH_2 terminus of SK is indicated by $I,^1$ and the COOH-terminal Lys^{414} is at the end of a long disordered segment (*squiggle*) of the γ-domain. During formation of the initial SK·Pg encounter complex (governed by K_1), Lys^{414} engages the LBS of K4, whereas the domains of SK are thought to not be fully engaged, and this does not produce a change in fluorescence. The first, tightening, conformational change governed by k_2 and k_{-2} with the largest decrease in fluorescence (*red triangle*) is shown hypothetically to involve insertion of SK Ile^1 into the NH_2-terminal binding cleft forming the Asp^{194} salt bridge and settling of the SK domains into a more ordered arrangement. The last conformational step controlled by k_3 and k_{-3} completes the arrangement of SK domains accompanied by a smaller fluorescence decrease (*maroon triangle*).

plasmin binding involves another SK lysine interacting with K5 in addition to Lys^{414} binding to K4. It is noteworthy that non-LBS interactions with the protease domain are significant sources of binding energy in both plasminogen and plasmin binding (71). Until now, SK binding to Pg had only been studied by equilibrium binding, and although the published K_D values report the affinities of the final complexes, they do not provide information on the intermediates in this multistep mechanism.

The results support the following sequential steps on the pathway to a stabilized complex with labeled Pg: SK Lys^{414} binding to a Pg kringle during formation of a weak, fluorescently silent encounter complex and two conformational steps of SK reorganization from a flexible to a more organized form during binding to the Pg protease domain accompanied by expression of a pro-exosite for binding of a second Pg molecule in the substrate mode. This reorganization is reported by biphasic fluorescence changes of the probe in the active site on the protease domain of Pg. Two striking differences between SK binding to labeled Pm and [Lys]Pg were immediately obvious: a ~40-fold weaker binding of SK in the encounter complex illustrated by higher SK concentrations required for saturation of the rates of fluorescence change and the requirement of stopped flow to study Pg displacement from the complex by FFR-Pm evidenced by the large increase in the off-rate constants k_{-2} and k_{-3}. Whereas displacement from the SK·Pm complex required several hours of incubation with excess FFR-Pm, the complexes with [Lys]Pg were easily reversed in a matter of seconds.

Binding to Pg also involves insertion of the NH_2 terminus of SK in the activation pocket of the Pg catalytic domain; however, adding a conformational step to the mechanism did not improve the fits. Stopped-flow fluorescence of SK binding to labeled Pg may not allow identifying the timing of the NH_2-terminal insertion or whether NH_2-terminal insertion contributes to the affinity of the Pg complex, and further studies are required to resolve this complex event.

Binding of SK Lys^{414} to a kringle facilitates formation of the encounter complexes with both [Lys]Pg and Pm as a similar 6–8-fold reduction in their affinity was observed when Lys^{414} was deleted. K_1 of the encounter complex with labeled [Lys]Pg increased from ~3 to ~19 μM upon deleting SK Lys^{414}. Saturation of the LBSs did not decrease the affinity of SK and SKΔK414 any further, indicating no other SK lysine-LBS interactions, and the 10–19 μM affinity range of LBS-blocked SK and SKΔK414 complexes likely represents the contribution of non-LBS binding to the Pg catalytic domain (Table 1). K_1 of the encounter complex with Pm increases from ~0.08 to ~0.67 μM upon SK Lys^{414} deletion (59); however, the SKΔK414·Pm encounter complex still exhibits substantial affinity, reflecting the sum of the LBS interactions with other lysine residues and non-LBS interactions with the protease domain. Kringle K5 harbors an LBS that preferentially interacts with ligands not carrying a free carboxylate function, such as alkylamines (51, 72, 73), and K5 on Pm may bind a non-COOH-terminal SK lysine. Saturation of Pm with 6-AHA disengages Lys^{414} and other lysines, and as expected, this affinity is not weakened further by SK Lys^{414} deletion. The remaining encounter affinity of ~5–8 μM likely represents the non-LBS interactions with the Pm catalytic domain (59). Multiple LBS interactions in the tighter encounter complex with Pm may be made possible by an increased flexibility of two-chain Pm compared with single chain Pg. This flexibility might also allow more intimate contacts during stabilization of the SK·Pm complex.

6-AHA binds kringles K1, K4, and K5, and the Pg binding results likely eliminate the involvement of K2 and K3 in SK Lys^{414} binding. Similarly, the weak SK binding to [Glu]Pg eliminates K1 as a candidate for Lys^{414} interaction as this is the only kringle in [Glu]Pg exposed for fibrin binding (74). Kringle K4 is not accessible in [Glu]Pg due to steric hindrance by the Pg NH_2-terminal PAN module, which binds K5 (75, 76). The identical encounter complex affinity of SK for [Glu]Pg in the absence and presence of 6-AHA indicated that LBS interactions do not play a role in [Glu]Pg binding.

Benzamidine blocks kringles K1, K2, and K5 and leaves kringle K4 available for lysine binding. The affinity of the SK·Pg encounter complex in 6-AHA and benzamidine was similar, suggesting that Lys^{414} binding to K4 in Pg does not increase the affinity when K5 is blocked. However, the SK·Pm encounter complex was ~2-fold tighter in benzamidine than that in 6-AHA and was further weakened by deletion of Lys^{414} (59). Further studies are required to clarify these different effects on Pg and Pm binding.

The 42-residue COOH-terminal sequence is not resolved in the SK·μPm crystal structure (19). Lys^{414} at the end of this disordered, mobile sequence may guide the pathway by initial interaction with the LBS on K4; however, this does not contribute much to the free energy of binding of the encounter complex. Calculating changes in free energy of association for SK

and SKΔK414 binding to Pg and Pm from $\Delta G^0 = RT \ln(K_D)$ using averaged K_1 values from Table 1 and our previous study (59) shows that the non-LBS interactions contribute ~83 and ~73% of the binding energy in Pg and Pm encounter complex formation, respectively. SK Lys^{414} contributes ~17 and ~13%. Binding of (an)other SK lysine residue(s) to Pm contributes ~14%. Although LBS interactions are important for efficient docking of SK, it appears that non-LBS interactions are the major source of the binding energy both for Pg and for Pm encounter. Previous equilibrium binding studies with α-domain-truncated SK showed that the LBS-independent interactions with the Pg/Pm protease domain largely reside in the SK α-domain, whereas the β- and γ-domains participate in LBS-dependent interactions with Pg/Pm kringles (71). It is likely that Pm-binding lysines other than the C-terminal Lys^{414} reside in the SK β- and γ-domains.

SK·Pg and SK·Pm differ in their rate constants for the two conformational steps. The k_2 values for the SK·Pm complex were ~10 s^{-1} for intact and Lys^{414}-deleted SK and ~37 s^{-1} in 6-AHA (59); the latter is comparable with k_2 for all the SK and SKΔK414 interactions with Pg in this study except those in benzamidine. For SK·Pm, the conformational restraint reflected by a low k_2 may be due to binding of a non-COOH-terminal SK lysine to K5, which also makes the SK·Pm encounter complex tighter. This restraint is absent in [Lys]Pg, suggesting no binding contribution from SK lysines other than Lys^{414}. Benzamidine enhanced k_2 by 5- and 6-fold in SK binding to Pg and Pm, respectively (59). This enhancement was weaker with SKΔK414, suggesting that Lys^{414} binding to K4 may release conformational restraints. The large k_2 value may contribute to a ~4-fold tighter $K_{D,\,\mathrm{overall}}$ for SK·Pg in benzamidine compared with that for SK·Pg in 6-AHA and SKΔK414·Pg in all buffer systems. 6-AHA causes transition of [Glu]Pg from the compact α-form to the fully extended γ-form and of [Lys]Pg from the partially extended β- to the γ-form, whereas benzamidine keeps [Lys]Pg in the β-form (43). This suggests that the release of constraints on k_2 does not depend on $\alpha \rightarrow \beta \rightarrow \gamma$ conformational changes in Pg. The k_{-2}, k_3, and k_{-3} values were similar in all data sets, indicating that these steps are LBS-independent.

In summary, we demonstrate here for the first time that the three-step kinetic model for the pathway of Pg binding to SK is substantially different from that of Pm binding with the main differences being a weaker encounter complex and increased off-rates for the conformational steps. Whereas cooperative Lys^{414} and other lysine interactions with K4 and K5 and non-LBS interactions with the protease domain contribute to formation of the SK·Pm complex, the SK·Pg* complex assembly appears to be driven by non-LBS interactions and by SK Lys^{414} binding to Pg kringle K4. Consistent with the experimentally determined K_m of ≥2 μM for substrate Pg binding to the SK·Pg* complex and of 270 nM for Pg binding to the SK·Pm complex (7) and in the absence of a crystal structure of the SK·Pg* complex, we hypothesize that the weaker interaction with Pg in the catalytic complex results in expression of a pro-exosite that binds substrate Pg with lower affinity than the corresponding exosite on the SK·Pm complex.

Differences in affinity of the SK·Pg* and SK·Pm complexes may be important in their partitioning on bacterial surface proteins and in binding to host fibrin(ogen). Group A streptococcal M-like surface proteins bind Pg with high affinity, and the M1 subset lacking Pm-binding motifs binds fibrinogen (Fbg). This allows indirect activation by way of SK·Pg*·Fbg ternary complex formation (7, 77), which proceeds by Fbg binding to the SK·Pg* complex rather than SK recruitment on the Pg·Fbg complex (7). Group A *Streptococcus* SK exhibits significant polymorphism (78–80), and considerable differences exist among SK allelic variants in their efficiency of activating Pg and their recruitment in complexes with Fbg, Fbg fragment D, fibrin, and the plasminogen-binding group A streptococcal M protein (81). [Glu]Pg binds fibrin(ogen) through a K1 interaction, whereas K1 and K4 of [Lys]Pg and Pm are involved in fibrin(ogen) binding (74), and these differences are expected to influence localization of SK·Pg* and SK·Pm complexes. Future stopped-flow studies will identify how fibrin(ogen) and streptococcal surface proteins affect the pathways of SK·Pg* and SK·Pm formation and will be instrumental in characterizing these pathways in complexes with allelic SK variants.

REFERENCES

1. Collen, D., and Lijnen, H. R. (1995) Molecular basis of fibrinolysis, as relevant for thrombolytic therapy. *Thromb. Haemost.* **74,** 167–171
2. Deryugina, E. I., and Quigley, J. P. (2012) Cell surface remodeling by plasmin: a new function for an old enzyme. *J. Biomed. Biotechnol.* **2012,** 564259
3. Carapetis, J. R., Steer, A. C., Mulholland, E. K., and Weber, M. (2005) The global burden of group A streptococcal diseases. *Lancet Infect. Dis.* **5,** 685–694
4. Preziuso, S., Laus, F., Tejeda, A. R., Valente, C., and Cuteri, V. (2010) Detection of *Streptococcus dysgalactiae* subsp. *equisimilis* in equine nasopharyngeal swabs by PCR. *J. Vet. Sci.* **11,** 67–72
5. Lopardo, H. A., Vidal, P., Sparo, M., Jeric, P., Centron, D., Facklam, R. R., Paganini, H., Pagniez, N. G., Lovgren, M., and Beall, B. (2005) Six-month multicenter study on invasive infections due to *Streptococcus pyogenes* and *Streptococcus dysgalactiae* subsp. *equisimilis* in Argentina. *J. Clin. Microbiol.* **43,** 802–807
6. Boxrud, P. D., and Bock, P. E. (2004) Coupling of conformational and proteolytic activation in the kinetic mechanism of plasminogen activation by streptokinase. *J. Biol. Chem.* **279,** 36642–36649
7. Nolan, M., Bouldin, S. D., and Bock, P. E. (2013) Full time course kinetics of the streptokinase-plasminogen activation pathway. *J. Biol. Chem.* **288,** 29482–29493
8. Boxrud, P. D., Verhamme, I. M., and Bock, P. E. (2004) Resolution of conformational activation in the kinetic mechanism of plasminogen activation by streptokinase. *J. Biol. Chem.* **279,** 36633–36641
9. McClintock, D. K., and Bell, P. H. (1971) The mechanism of activation of human plasminogen by streptokinase. *Biochem. Biophys. Res. Commun.* **43,** 694–702
10. Wohl, R. C., Summaria, L., Arzadon, L., and Robbins, K. C. (1978) Steady state kinetics of activation of human and bovine plasminogens by streptokinase and its equimolar complexes with various activated forms of human plasminogen. *J. Biol. Chem.* **253,** 1402–1407
11. Reddy, K. N., and Markus, G. (1972) Mechanism of activation of human plasminogen by streptokinase. Presence of active center in streptokinase-plasminogen complex. *J. Biol. Chem.* **247,** 1683–1691
12. Schick, L. A., and Castellino, F. J. (1974) Direct evidence for the generation of an active site in the plasminogen moiety of the streptokinase-human plasminogen activator complex. *Biochem. Biophys. Res. Commun.* **57,** 47–54
13. Bajaj, A. P., and Castellino, F. J. (1977) Activation of human plasminogen by equimolar levels of streptokinase. *J. Biol. Chem.* **252,** 492–498
14. Davidson, D. J., Higgins, D. L., and Castellino, F. J. (1990) Plasminogen activator activities of equimolar complexes of streptokinase with variant

recombinant plasminogens. *Biochemistry* **29,** 3585–3590
15. Boxrud, P. D., Verhamme, I. M., Fay, W. P., and Bock, P. E. (2001) Streptokinase triggers conformational activation of plasminogen through specific interactions of the amino-terminal sequence and stabilizes the active zymogen conformation. *J. Biol. Chem.* **276,** 26084–26089
16. Wang, S., Reed, G. L., and Hedstrom, L. (1999) Deletion of Ile1 changes the mechanism of streptokinase: evidence for the molecular sexuality hypothesis. *Biochemistry* **38,** 5232–5240
17. Wang, S., Reed, G. L., and Hedstrom, L. (2000) Zymogen activation in the streptokinase-plasminogen complex. Ile1 is required for the formation of a functional active site. *Eur. J. Biochem.* **267,** 3994–4001
18. Bode, W., and Huber, R. (1976) Induction of the bovine trypsinogen-trypsin transition by peptides sequentially similar to the N-terminus of trypsin. *FEBS Lett.* **68,** 231–236
19. Wang, X., Lin, X., Loy, J. A., Tang, J., and Zhang, X. C. (1998) Crystal structure of the catalytic domain of human plasmin complexed with streptokinase. *Science* **281,** 1662–1665
20. Friedrich, R., Panizzi, P., Fuentes-Prior, P., Richter, K., Verhamme, I., Anderson, P. J., Kawabata, S., Huber, R., Bode, W., and Bock, P. E. (2003) Staphylocoagulase is a prototype for the mechanism of cofactor-induced zymogen activation. *Nature* **425,** 535–539
21. Kroh, H. K., and Bock, P. E. (2012) Effect of zymogen domains and active site occupation on activation of prothrombin by von Willebrand factor-binding protein. *J. Biol. Chem.* **287,** 39149–39157
22. Malke, H., and Steiner, K. (2004) Control of streptokinase gene expression in group A & C streptococci by two-component regulators. *Indian J. Med. Res.* **119,** (suppl.) 48–56
23. Walker, M. J., McArthur, J. D., McKay, F., and Ranson, M. (2005) Is plasminogen deployed as a *Streptococcus pyogenes* virulence factor? *Trends Microbiol.* **13,** 308–313
24. Sun, H., Ringdahl, U., Homeister, J. W., Fay, W. P., Engleberg, N. C., Yang, A. Y., Rozek, L. S., Wang, X., Sjöbring, U., and Ginsburg, D. (2004) Plasminogen is a critical host pathogenicity factor for group A streptococcal infection. *Science* **305,** 1283–1286
25. Khil, J., Im, M., Heath, A., Ringdahl, U., Mundada, L., Cary Engleberg, N., and Fay, W. P. (2003) Plasminogen enhances virulence of group A streptococci by streptokinase-dependent and streptokinase-independent mechanisms. *J. Infect. Dis.* **188,** 497–505
26. Boxrud, P. D., Fay, W. P., and Bock, P. E. (2000) Streptokinase binds to human plasmin with high affinity, perturbs the plasmin active site, and induces expression of a substrate recognition exosite for plasminogen. *J. Biol. Chem.* **275,** 14579–14589
27. Boxrud, P. D., and Bock, P. E. (2000) Streptokinase binds preferentially to the extended conformation of plasminogen through lysine binding site and catalytic domain interactions. *Biochemistry* **39,** 13974–13981
28. Damaschun, G., Damaschun, H., Gast, K., Gerlach, D., Misselwitz, R., Welfle, H., and Zirwer, D. (1992) Streptokinase is a flexible multi-domain protein. *Eur. Biophys. J.* **20,** 355–361
29. Henkin, J., Marcotte, P., and Yang, H. C. (1991) The plasminogen-plasmin system. *Prog. Cardiovasc. Dis.* **34,** 135–164
30. Ponting, C. P., Marshall, J. M., and Cederholm-Williams, S. A. (1992) Plasminogen: a structural review. *Blood Coagul. Fibrinolysis* **3,** 605–614
31. Law, R. H., Caradoc-Davies, T., Cowieson, N., Horvath, A. J., Quek, A. J., Encarnacao, J. A., Steer, D., Cowan, A., Zhang, Q., Lu, B. G., Pike, R. N., Smith, A. I., Coughlin, P. B., and Whisstock, J. C. (2012) The x-ray crystal structure of full-length human plasminogen. *Cell Rep.* **1,** 185–190
32. Marti, D. N., Hu, C. K., An, S. S., von Haller, P., Schaller, J., and Llinás, M. (1997) Ligand preferences of kringle 2 and homologous domains of human plasminogen: canvassing weak, intermediate, and high-affinity binding sites by ^{1}H-NMR. *Biochemistry* **36,** 11591–11604
33. Castellino, F. J., and McCance, S. G. (1997) The kringle domains of human plasminogen. *Ciba Found. Symp.* **212,** 46–60; discussion 60–65
34. Christensen, U. (1985) C-terminal lysine residues of fibrinogen fragments essential for binding to plasminogen. *FEBS Lett.* **182,** 43–46
35. Lucas, M. A., Fretto, L. J., and McKee, P. A. (1983) The binding of human plasminogen to fibrin and fibrinogen. *J. Biol. Chem.* **258,** 4249–4256
36. Wiman, B., Lijnen, H. R., and Collen, D. (1979) On the specific interaction between the lysine-binding sites in plasmin and complementary sites in α2-antiplasmin and in fibrinogen. *Biochim. Biophys. Acta* **579,** 142–154
37. Bok, R. A., and Mangel, W. F. (1985) Quantitative characterization of the binding of plasminogen to intact fibrin clots, lysine-Sepharose, and fibrin cleaved by plasmin. *Biochemistry* **24,** 3279–3286
38. Clemmensen, I., Petersen, L. C., and Kluft, C. (1986) Purification and characterization of a novel, oligomeric, plasminogen kringle 4 binding protein from human plasma: tetranectin. *Eur. J. Biochem.* **156,** 327–333
39. Marshall, J. M., Brown, A. J., and Ponting, C. P. (1994) Conformational studies of human plasminogen and plasminogen fragments: evidence for a novel third conformation of plasminogen. *Biochemistry* **33,** 3599–3606
40. Mangel, W. F., Lin, B. H., and Ramakrishnan, V. (1990) Characterization of an extremely large, ligand-induced conformational change in plasminogen. *Science* **248,** 69–73
41. Ponting, C. P., Holland, S. K., Cederholm-Williams, S. A., Marshall, J. M., Brown, A. J., Spraggon, G., and Blake, C. C. (1992) The compact domain conformation of human Glu-plasminogen in solution. *Biochim. Biophys. Acta* **1159,** 155–161
42. Weisel, J. W., Nagaswami, C., Korsholm, B., Petersen, L. C., and Suenson, E. (1994) Interactions of plasminogen with polymerizing fibrin and its derivatives, monitored with a photoaffinity cross-linker and electron microscopy. *J. Mol. Biol.* **235,** 1117–1135
43. Cockell, C. S., Marshall, J. M., Dawson, K. M., Cederholm-Williams, S. A., and Ponting, C. P. (1998) Evidence that the conformation of unliganded human plasminogen is maintained via an intramolecular interaction between the lysine-binding site of kringle 5 and the N-terminal peptide. *Biochem. J.* **333,** 99–105
44. Hoylaerts, M., Rijken, D. C., Lijnen, H. R., and Collen, D. (1982) Kinetics of the activation of plasminogen by human tissue plasminogen activator. Role of fibrin. *J. Biol. Chem.* **257,** 2912–2919
45. Wohl, R. C., Summaria, L., and Robbins, K. C. (1980) Kinetics of activation of human plasminogen by different activator species at pH 7.4 and 37 °C. *J. Biol. Chem.* **255,** 2005–2013
46. Violand, B. N., Byrne, R., and Castellino, F. J. (1978) The effect of α-,ω-amino acids on human plasminogen structure and activation. *J. Biol. Chem.* **253,** 5395–5401
47. Violand, B. N., and Castellino, F. J. (1976) Mechanism of the urokinase-catalyzed activation of human plasminogen. *J. Biol. Chem.* **251,** 3906–3912
48. Panizzi, P., Boxrud, P. D., Verhamme, I. M., and Bock, P. E. (2006) Binding of the COOH-terminal lysine residue of streptokinase to plasmin(ogen) kringles enhances formation of the streptokinase·plasmin(ogen) catalytic complexes. *J. Biol. Chem.* **281,** 26774–26778
49. Lerch, P. G., Rickli, E. E., Lergier, W., and Gillessen, D. (1980) Localization of individual lysine-binding regions in human plasminogen and investigations on their complex-forming properties. *Eur. J. Biochem.* **107,** 7–13
50. Markus, G., DePasquale, J. L., and Wissler, F. C. (1978) Quantitative determination of the binding of ϵ-aminocaproic acid to native plasminogen. *J. Biol. Chem.* **253,** 727–732
51. Thewes, T., Constantine, K., Byeon, I. J., and Llinás, M. (1990) Ligand interactions with the kringle 5 domain of plasminogen. A study by ^{1}H NMR spectroscopy. *J. Biol. Chem.* **265,** 3906–3915
52. Váradi, A., and Patthy, L. (1981) Kringle 5 of human plasminogen carries a benzamidine-binding site. *Biochem. Biophys. Res. Commun.* **103,** 97–102
53. Christensen, U., and Mølgaard, L. (1992) Positive co-operative binding at two weak lysine-binding sites governs the Glu-plasminogen conformational change. *Biochem. J.* **285,** 419–425
54. Bock, P. E. (1992) Active-site-selective labeling of blood coagulation proteinases with fluorescence probes by the use of thioester peptide chloromethyl ketones. I. Specificity of thrombin labeling. *J. Biol. Chem.* **267,** 14963–14973
55. Bock, P. E. (1992) Active-site-selective labeling of blood coagulation proteinases with fluorescence probes by the use of thioester peptide chloromethyl ketones. II. Properties of thrombin derivatives as reporters of prothrombin fragment 2 binding and specificity of the labeling approach for other proteinases. *J. Biol. Chem.* **267,** 14974–14981
56. Verhamme, I. M., Olson, S. T., Tollefsen, D. M., and Bock, P. E. (2002) Binding of exosite ligands to human thrombin. Re-evaluation of allosteric linkage between thrombin exosites I and II. *J. Biol. Chem.* **277,** 6788–6798

57. Panizzi, P., Friedrich, R., Fuentes-Prior, P., Kroh, H. K., Briggs, J., Tans, G., Bode, W., and Bock, P. E. (2006) Novel fluorescent prothrombin analogs as probes of staphylocoagulase-prothrombin interactions. *J. Biol. Chem.* **281,** 1169–1178
58. Bock, P. E., Day, D. E., Verhamme, I. M., Bernardo, M. M., Olson, S. T., and Shore, J. D. (1996) Analogs of human plasminogen that are labeled with fluorescence probes at the catalytic site of the zymogen. Preparation, characterization, and interaction with streptokinase. *J. Biol. Chem.* **271,** 1072–1080
59. Verhamme, I. M., and Bock, P. E. (2008) Rapid-reaction kinetic characterization of the pathway of streptokinase-plasmin catalytic complex formation. *J. Biol. Chem.* **283,** 26137–26147
60. Deutsch, D. G., and Mertz, E. T. (1970) Plasminogen: purification from human plasma by affinity chromatography. *Science* **170,** 1095–1096
61. Castellino, F. J., and Powell, J. R. (1981) Human plasminogen. *Methods Enzymol.* **80,** 365–378
62. Bock, P. E., Craig, P. A., Olson, S. T., and Singh, P. (1989) Isolation of human blood coagulation a-factor Xa by soybean trypsin inhibitor-Sepharose chromatography and its active-site titration with fluorescein mono-p-guanidinobenzoate. *Arch. Biochem. Biophys.* **273,** 375–388
63. Laha, M., Panizzi, P., Nahrendorf, M., and Bock, P. E. (2011) Engineering streptokinase for generation of active site-labeled plasminogen analogs. *Anal. Biochem.* **415,** 105–115
64. Sjöholm, I. (1973) Studies on the conformational changes of plasminogen induced during activation to plasmin and by 6-aminohexanoic acid. *Eur. J. Biochem.* **39,** 471–479
65. Taylor, F. B., Jr., and Botts, J. (1968) Purification and characterization of streptokinase with studies of streptokinase activation of plasminogen. *Biochemistry* **7,** 232–242
66. Jackson, K. W., and Tang, J. (1982) Complete amino acid sequence of streptokinase and its homology with serine proteases. *Biochemistry* **21,** 6620–6625
67. Johnson, K. A. (2009) Fitting enzyme kinetic data with KinTek Global Kinetic Explorer. *Methods Enzymol.* **467,** 601–626
68. Johnson, K. A., Simpson, Z. B., and Blom, T. (2009) FitSpace explorer: an algorithm to evaluate multidimensional parameter space in fitting kinetic data. *Anal. Biochem.* **387,** 30–41
69. Johnson, K. A., Simpson, Z. B., and Blom, T. (2009) Global kinetic explorer: a new computer program for dynamic simulation and fitting of kinetic data. *Anal. Biochem.* **387,** 20–29
70. Tsodikov, O. V., and Record, M. T., Jr. (1999) General method of analysis of kinetic equations for multistep reversible mechanisms in the single-exponential regime: application to kinetics of open complex formation between Eσ70 RNA polymerase and λP(R) promoter DNA. *Biophys. J.* **76,** 1320–1329
71. Bean, R. R., Verhamme, I. M., and Bock, P. E. (2005) Role of the streptokinase α-domain in the interactions of streptokinase with plasminogen and plasmin. *J. Biol. Chem.* **280,** 7504–7510
72. Chang, Y., Mochalkin, I., McCance, S. G., Cheng, B., Tulinsky, A., and Castellino, F. J. (1998) Structure and ligand binding determinants of the recombinant kringle 5 domain of human plasminogen. *Biochemistry* **37,** 3258–3271
73. Christensen, U. (1984) The AH-site of plasminogen and two C-terminal fragments. A weak lysine-binding site preferring ligands not carrying a free carboxylate function. *Biochem. J.* **223,** 413–421
74. Ho-Tin-Noé, B., Rojas, G., Vranckx, R., Lijnen, H. R., and Anglés-Cano, E. (2005) Functional hierarchy of plasminogen kringles 1 and 4 in fibrinolysis and plasmin-induced cell detachment and apoptosis. *FEBS J.* **272,** 3387–3400
75. Váli, Z., and Patthy, L. (1982) Location of the intermediate and high affinity ω-aminocarboxylic acid-binding sites in human plasminogen. *J. Biol. Chem.* **257,** 2104–2110
76. McCance, S. G., and Castellino, F. J. (1995) Contributions of individual kringle domains toward maintenance of the chloride-induced tight conformation of human glutamic acid-1 plasminogen. *Biochemistry* **34,** 9581–9586
77. Sanderson-Smith, M. L., Walker, M. J., and Ranson, M. (2006) The maintenance of high affinity plasminogen binding by group A streptococcal plasminogen-binding M-like protein is mediated by arginine and histidine residues within the a1 and a2 repeat domains. *J. Biol. Chem.* **281,** 25965–25971
78. Cook, S. M., Skora, A., Gillen, C. M., Walker, M. J., and McArthur, J. D. (2012) Streptokinase variants from *Streptococcus pyogenes* isolates display altered plasminogen activation characteristics: implications for pathogenesis. *Mol. Microbiol.* **86,** 1052–1062
79. Kalia, A., and Bessen, D. E. (2004) Natural selection and evolution of streptococcal virulence genes involved in tissue-specific adaptations. *J. Bacteriol.* **186,** 110–121
80. Zhang, Y., Liang, Z., Hsueh, H. T., Ploplis, V. A., and Castellino, F. J. (2012) Characterization of streptokinases from group A streptococci reveals a strong functional relationship that supports the coinheritance of plasminogen-binding M protein and cluster 2b streptokinase. *J. Biol. Chem.* **287,** 42093–42103
81. Cook, S. M., Skora, A., Walker, M. J., Sanderson-Smith, M. L., and McArthur, J. D. (2014) Site-restricted plasminogen activation mediated by group A streptococcal streptokinase variants. *Biochem. J.* **458,** 23–31